Research Article
Viral Hepatitis

JOURNAL
OF HEPATOLOGY

Fibrogenic signals persist in DAA-treated HCV patients after sustained virological response

Graphical abstract

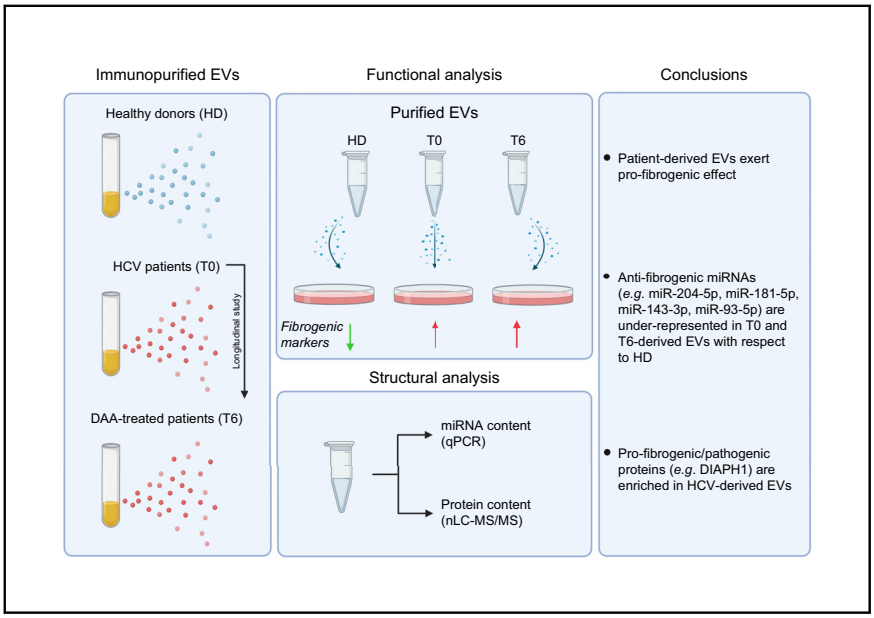

Highlights

- HCV T0/T6 EVs have been functionally and structurally compared to HD EVs.
- HD EVs ameliorate LX2 cells' fibrogenic phenotype while HCV T0/T6 EVs do not.
- HCV T0/T6 EVs contain lower levels of antifibrogenic miRNAs compared to HD EVs.
- HCV T0/T6 EVs' cargo is enriched in profibrogenic proteins (*e.g.* DIAPH1).
- SVR does not restore antifibrogenic cargo and activity in HCV EVs.

Authors

Claudia Montaldo, Michela Terri, Veronica Riccioni, …, Raffaele Strippoli, Chiara Agrati, Marco Tripodi

Correspondence

marco.tripodi@uniroma1.it (M. Tripodi).

Lay summary

Direct-acting antivirals lead to virological cure in the majority of patients with chronic hepatitis C virus infection. However, the risk of liver disease progression or complications in patients with fibrosis and cirrhosis remains in some patients even after virological cure. Herein, we show that extracellular vesicle modifications could be linked to long-term liver disease progression in patients who have achieved virological cure; these modifications could potentially be used as biomarkers or treatment targets in such patients.

https://doi.org/10.1016/j.jhep.2021.07.003
 J. Hepatol. 2021, 75, 1301–1311

Research Article
Viral Hepatitis

JOURNAL OF HEPATOLOGY

Fibrogenic signals persist in DAA-treated HCV patients after sustained virological response

Claudia Montaldo[1,#], Michela Terri[1,2,#], Veronica Riccioni[2], Cecilia Battistelli[2], Veronica Bordoni[1], Gianpiero D'Offizi[1], Maria Giulia Prado[2], Flavia Trionfetti[1,2], Tiziana Vescovo[1], Eleonora Tartaglia[1], Raffaele Strippoli[1,2], Chiara Agrati[1], Marco Tripodi[1,2,*]

[1]*National Institute for Infectious Diseases L. Spallanzani, IRCCS, Italy;* [2]*Istituto Pasteur Italia-Fondazione Cenci Bolognetti, Department of Molecular Medicine, Sapienza University of Rome, Rome, Italy*

Background & Aims: Patients with HCV who achieve a sustained virological response (SVR) on direct-acting antiviral (DAA) therapy still need to be monitored for signs of liver disease progression. To this end, the identification of both disease biomarkers and therapeutic targets is necessary.

Methods: Extracellular vesicles (EVs) purified from plasma of 15 healthy donors (HDs), and 16 HCV-infected patients before (T0) and after (T6) DAA treatment were utilized for functional and miRNA cargo analysis. EVs purified from plasma of 17 HDs and 23 HCV-infected patients (T0 and T6) were employed for proteomic and western blot analyses. Functional analysis in LX2 cells measured fibrotic markers (mRNAs and proteins) in response to EVs. Structural analysis was performed by qPCR, label-free liquid chromatography-mass spectrometry and western blot.

Results: On the basis of observations indicating functional differences (*i.e.* modulation of FN-1, ACTA2, Smad2/3 phosphorylation, collagen deposition) of plasma-derived EVs from HDs, T0 and T6, we performed structural analysis of EVs. We found consistent differences in terms of both miRNA and protein cargos: (i) antifibrogenic miR204-5p, miR181a-5p, miR143-3p, miR93-5p and miR122-5p were statistically underrepresented in T0 EVs compared to HD EVs, while miR204-5p and miR143-3p were statistically underrepresented in T6 EVs compared to HD EVs (p <0.05); (ii) proteomic analysis highlighted, in both T0 and T6, the modulation of several proteins with respect to HDs; among them, the fibrogenic protein DIAPH1 was upregulated (Log_2 fold change of 4.4).

Conclusions: Taken together, these results highlight structural EV modifications that are conceivably causal for long-term liver disease progression in patients with HCV despite DAA-mediated SVR.

Lay summary: Direct-acting antivirals lead to virological cure in the majority of patients with chronic hepatitis C virus infection. However, the risk of liver disease progression or complications in patients with fibrosis and cirrhosis remains in some patients even after virological cure. Herein, we show that extracellular vesicle modifications could be linked to long-term liver disease progression in patients who have achieved virological cure; these modifications could potentially be used as biomarkers or treatment targets in such patients.

Introduction

New direct-acting antiviral (DAA)-based therapy, available with first-generation compounds since 2011, efficiently eradicates HCV, thus providing a therapeutic opportunity for 71 million people (WHO estimated) affected by chronic HCV infection who would otherwise eventually develop cirrhosis or liver cancer.[1] HCV elimination does not always result in the cure of liver disease, particularly in patients with advanced fibrosis or cirrhosis; emerging clinical studies with DAAs in patients with cirrhosis stirred a heated debate about the risk of hepatocellular carcinoma (HCC) occurrence and recurrence after viral cure.[2–4] In this scenario, early non-invasive prognostic tools that can assess long-term post-DAA clinical outcomes appear necessary to guide patient management. Recently, the scientific community has focused on circulating extracellular vesicles (EVs) for 2 reasons: i) EV-delivered biological messages may be causally associated with disease progression and ii) their analysis may provide prognostic and diagnostic information. Current technologies enable EV analysis for both informational content (*i.e.* DNA, mRNAs, microRNAs, long non-coding RNAs and proteins) and functional analysis, assessed by means of target cell response. In fact, EV analysis has already proven clinically useful, as in the case of Epstein-Barr virus (EBV)-associated tumors, where it was found that circulating EV cargo may include EBV miR-BART2-5p, a diagnostic and prognostic biomarker functionally able to protect latent cells from EBV reactivation.[5] Similarly, in antiretroviral therapy-treated patients with HIV, EVs were found to carry proteins related to immune activation and oxidative stress that had functional immunomodulatory effects.[6] Specifically in the frame of DAA therapy, it has previously been described that the expression of specific microRNAs (miRNAs) present in EVs is modulated by this therapy, as these changes correlate with the EV-mediated natural killer cell degranulation capability.[7]

In this study, we assess the impact of DAA therapy on liver fibrosis progression, analyzing the functional abilities and the

Keywords: Fibrosis; HCV; DAA; Extracellular vesicles; miRNAs; Proteomics; nLC-MS/MS; DIAPH1; miR204-5p; miR181a-5p; miR93-5p; miR143-3p.
Received 21 December 2020; received in revised form 22 June 2021; accepted 1 July 2021; available online 13 July 2021

* Corresponding author. Address: Department of Molecular Medicine, Sapienza, University of Rome, Viale Regina Elena 324, Rome 00161, Italy. Tel. +390649918244, fax: +39064462891.
E-mail address: marco.tripodi@uniroma1.it (M. Tripodi).
[#] These authors equally contributed

https://doi.org/10.1016/j.jhep.2021.07.003

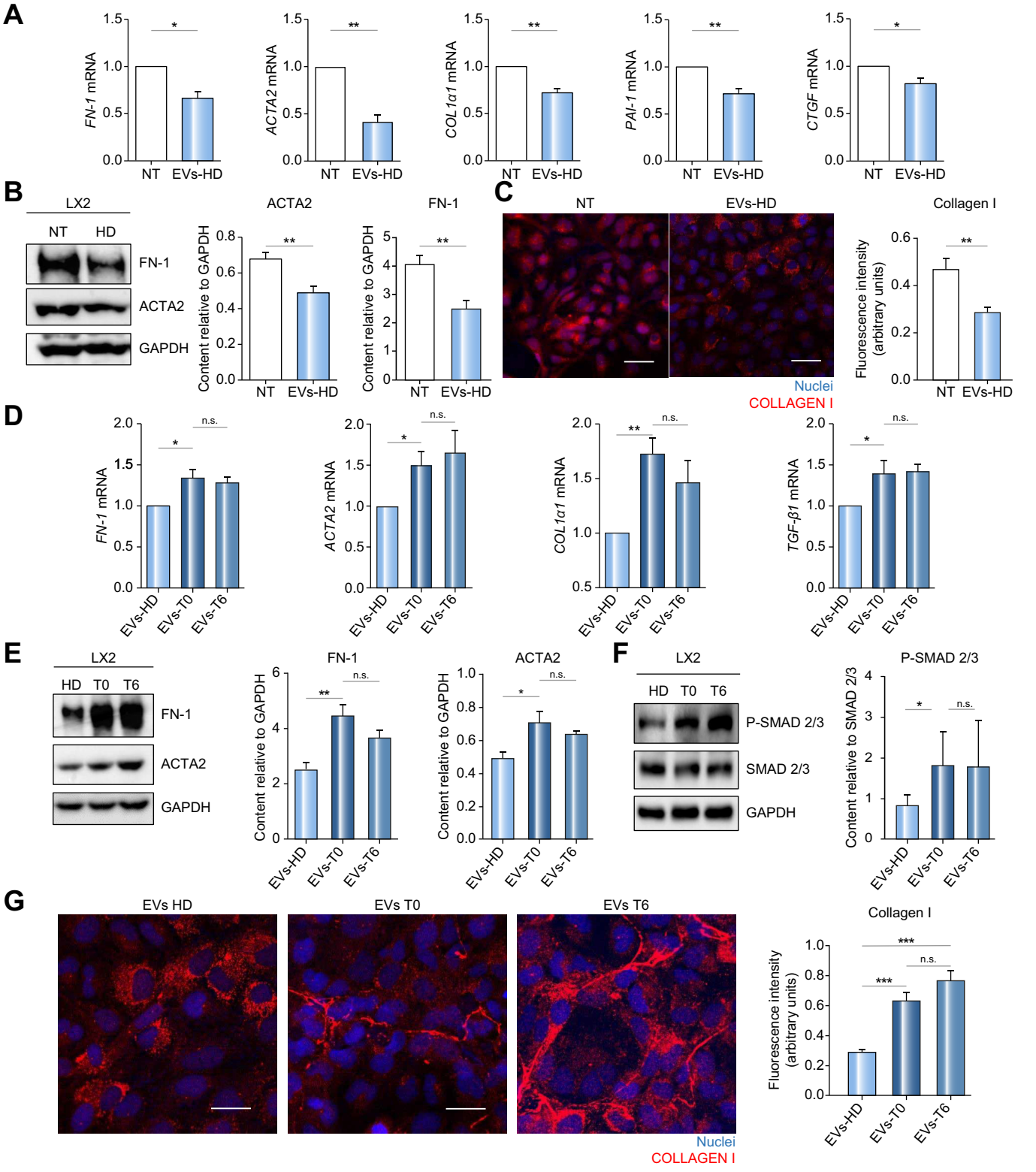

Fig. 1. EVs derived from HDs limit the fibrogenic phenotype in LX2 cells whereas EVs derived from T0/T6 HCV patients maintain it. (A-C) HD EVs limit the fibrogenic phenotype in LX2 cells. Fibrogenic markers were compared in untreated LX2 cells (NT) and LX2 cells after incubation with EVs (relative to 20 μg of total protein) from HDs. (A) RT-qPCR analysis for the indicated markers. The values are calculated by the ΔΔCt method and expressed relative to the *RPL34* RNA expression. (B) (left panel) representative WB analysis for the indicated proteins; (right panel) densitometric analysis of WB signals; data are shown as mean ± SEM of 5 independent experiments. GAPDH was used as a loading control. (C) (left) Immunofluorescence for collagen I. Nuclei were stained with Draq5. Images are representative of 3 independent experiments. (right) Quantification of collagen I intensity. A minimum of 4 fields per sample (at least 150 total cells per sample) from 3 independent experiments were analyzed. Signal intensity, quantified using the ImageJ software, was normalized to the number of nuclei present in each field. Histogram shows the mean fluorescence intensity ± SEM. $^{**}p$ <0.01. Scale bar: 30 μm. (D-G) T0/T6 HCV EVs maintain fibrogenic phenotype.

structure of circulating EVs derived from HCV-infected and DAA-cleared patients.

Functional EV analysis was performed on LX2 cells, a hepatic stellate cell (HSC)/myofibroblast cell line partially mimicking the highly proliferative myofibroblast-like cells that derive from quiescent HSCs. Indeed, during chronic HCV infection, HSCs transition into highly proliferative myofibroblast-like cells expressing inflammatory and fibrogenic mediators responsible for extracellular matrix (ECM) accumulation within the micro-environment, thus contributing to the fibrotic process that leads to cirrhosis and liver failure in advanced stages.[8,9]

EV structural analysis was performed for both miRNA and protein content. Data obtained show that EVs derived from HCV-infected patients, with respect to EVs derived from healthy donors (HDs), increase the fibrogenic activity of the LX2 cell line and that this functional data correlates with upregulation of HSC activators (*e.g.* of DIAPH1) and downregulation of some anti-fibrogenic miRNAs (*e.g.* miR204-5p, miR93-5p, miR143-3p, miR181a-5p and miR122-5p). Notably, longitudinal analysis highlights the persistent pro-fibrogenic activity of EVs despite DAA-mediated HCV eradication; this again correlates with the EV informational content: upregulation of DIAPH1 and down-regulation of miR204-5p and miR143-3p.

Materials and methods

Patient selection

This study received the approval of the I.R.C.C.S. National Institute for Infectious Diseases L. Spallanzani Ethics Committee, Rome, Italy. Written informed consent for plasma donation to our biobank was obtained from all patients and HDs. The authors confirm that all experiments were performed in accordance with the relevant guidelines and regulations. A total of 39 naïve chronic HCV-infected patients were enrolled for a longitudinal study performed before (T0) and after 6 months of DAA therapy (T6); at T6 all enrolled patients achieved sustained virological response (SVR), defined as undetectable HCV RNA. 32 HD were included as controls. Their characteristics are shown in Table S1.

HCV RNA detection

HCV RNA plasma quantification was measured using the ABBOTT Real-Time HCV Assay (ABBOTT Molecular Inc., Des Plaines, IL, USA) with a reported lower limit of quantification = 12 IU/ml.

Blood sampling

Peripheral blood in K2-Ethylenediaminetetraacetic acid (EDTA) BD Vacutainer® blood collection tubes (BD Biosciences, Franklin Lakes, NJ, USA) was centrifuged at 3,500 g for 15 minutes to obtain the plasma, then aliquoted and stored at INMI Biobank at −80 °C until EV purification.

Extracellular vesicle purification

The isolation of plasma/cell-derived EVs was performed by positive selection using microbeads recognizing the tetraspanin proteins CD9, CD63 and CD81 following manufacturer's instructions (Miltenyi Biotec, BG, Germany). Briefly, 1 ml of plasma sample/cell conditioned medium was centrifuged at 2,000 g for 30 minutes and at 10,000 g for 45 minutes to remove cell debris and larger vesicles. After EV labeling with microbeads, EVs contained in the sample were firstly magnetically separated and used in subsequent investigations.

Cell culture, EV incubation, IF and western blot analysis

The human HSC line (LX2) and tumor cell line HepG2 were cultured in DMEM (Gibco, Grand Island, NY, USA) supplemented with 10% FBS (Gibco), glutamine, and 1% penicillin-streptomycin. Non-tumorigenic murine hepatocyte 3A cells were grown as in.[10] LX2 cells were incubated with EVs purified from HDs, HCV T0/T6 plasma samples or HEPG2/3A-conditioned media at 37 °C in a humidified 5% CO_2 atmosphere for 72 h (protein detection), 48 h (mRNA detection) or 6 h (phospho-SMAD protein detection). Western blot analysis was performed as previously described.[7] For immunofluorescence experiments, LX2 cells treated as above were fixed with 4% paraformaldehyde (Sigma-Aldrich, St. Louis, MO, USA) in PBS for 20 minutes and permeabilized with 0.2% Triton X-100 (Sigma-Aldrich) in PBS for 5 minutes. Coverslips were mounted in Prolong Gold antifade (Life Technologies, Carlsbad, CA, USA) and acquired using a confocal microscope (Leica TCS SP2, Wetzlar, Germany) using a 63x objective. A minimum of 4 fields per sample (at least 150 total cells per sample) from 3 independent experiments were analyzed.

The primary antibodies used in this study were: FN-1, DIAPH1 and SDCBP (Abcam, Cambridge, UK); FLOT-1, CD9 and CLX (Santa Cruz Biotechnology, Dallas, Texas, USA); ACTA2 (Sigma-Aldrich); ANXA7 (BD Biosciences); GAPDH (Calbiochem-Merck Darmstadt, Germany); Alix, SMAD-2/3 and P-SMAD-2/3 (Cell Signaling Danvers, MA, USA); collagen I (Novus Biological, Litterton, CO, USA). Cy3/Peroxidase-conjugated secondary antibody (Jackson Immunoresearch, Philadelphia, PA, USA). DRAQ5 to visualize nuclei (Miltenyi Biotec).

RNA extraction and quantification by real-time PCR

EVs from 5 HDs and 5 T0/T6 donors were used. Unprotected RNA was degraded by 15 minutes incubation with 2 mg/ml of protease-free RNase A (Sigma-Aldrich) followed by the addition of RNAsin® ribonuclease inhibitor (Promega, Madison, WI, USA). RNA extraction, RNA quantification, retrotranscription and amplification were performed as in.[7] Relative expression of 12 miRNAs (miR-204-5p, miR-93-5p, miR-181a-5p, miR-143-3p, miR122-5p, miR-199a-5p, miR-484, miR-320a, miR-486, miR-93-3p, miR-145-5p, miR-199a-3p) was determined by the comparative threshold (ΔCt) method (ΔCt = Ct target gene−Ct reference gene) and expressed as $2^{-(-\Delta Ct)}$, using the geometric mean[11,12] of miR-22-5p, miR191 and miR-26a-5p Ct-values as the reference normalization factor. Primers are listed in Table S2.

For gene expression analysis, EV-treated LX2 total RNA was extracted with TRIzol® Reagent (Life Technologies), reverse

Fibrogenic markers were analyzed in LX2 cells after incubation with EVs (relative to 20 μg of total protein) from HDs or T0/T6 HCV. (D) RT-qPCR analysis for the indicated markers measured as in (A) (n = 5). (E) WB (left) and densitometric analysis (right) of the indicated proteins measured as in (B) (n = 5). (F) Western blot and densitometric analysis of p-SMAD2/3 and SMAD2/3 as in (E) (n = 3). (G) (left) Immunofluorescence for collagen I. Nuclei were stained with Draq5. Images are representative of 3 independent experiments. (right): Quantification of collagen I intensity quantified as in Fig. 1C. Histogram shows the mean fluorescence intensity ± SEM. ***p <0.001. Scale bar: 17 μm. Statistical analysis was performed by Student's t test. p <0.05 is considered statistically significant. EVs, extracellular vesicles; HDs, healthy donors; RT-qPCR, reverse-transcription quantitative PCR; WB, western blot.

Table 1. Anti-fibrogenic miRNAs analyzed in this study.

MicroRNAs	miRBase ID	Target	Target genes validated by mimics
hsa-miR-204-5p	MIMAT0000265	*TGFβR2, ZEB1, TGFβR2, Snail2*	*COL1α1, TGFβ1, TGFβ1R1, CTGF*
hsa-miR-181a-5p	MIMAT0000256	*TGFβR1*	*FN1, ACTA2, COL1α1, TGFβ1R1, CTGF*
hsa-miR-143-3p	MIMAT0000435	*NFATc1, CTGF*	*COL1α1, TGFβ1R1, CTGF*
hsa-miR-93-5p	MIMAT0000093	*Orai1*	*FN1, ACTA2, COL1α1, TGFβ1,TGFβ1R1, CTGF*
hsa-miR-199a-5p	MIMAT0000231	*CTGF*	
hsa-miR-484-5p	MIMAT0002174	*TGFβR3* predicted	
hsa-miR-199a-3p	MIMAT0000232	*Snail*	
hsa-miR-486-5p	MIMAT0002177	*SMAD2*	
hsa-miR-320a-3p	MIMAT0037311	*SRF*	
hsa-miR-93-3p	MIMAT0004509	*TGFβR2*	
hsa-miR-145-5p	MIMAT0000437	*SMAD2, SMAD3, ZEB2*	
hsa-miR-122-5p	MIMAT0000421	*TGFβR2/SMAD4*	

List of miRNAs analyzed with their direct/indirect target genes and the relative references; direct/indirect target genes validated by mimics are listed in the last column.

transcription was performed with AMV Reverse Transcriptase (Promega) and quantitative PCR (qPCR) was performed with Maxima SYBR Green/ROX qPCR Master Mix (Thermo Fisher Scientific, Waltham, MA, USA). Relative expression levels were calculated with the 2-(-ΔΔCt) method and were normalized to L34 ribosomal RNA. qPCR reactions were performed in a Corbett 212 Rotor-gene 6000 Real-Time PCR System (Qiagen). Primers are listed in Table S3.

Protein digestion, peptide purification and nanoLC analysis

EVs purified from HDs and HCV T0/T6 samples (n = 3) were lysed in RIPA Buffer and quantified by Bradford assay. 15 ug of protein extract per sample were treated with DL-Dithiothreitol (10 mM at 56 °C) and Iodoacetamide (55 mM at RT) for disulfide bond reduction and alkylation, respectively. After 100% ethanol precipitation, samples were resuspended in 50 mM NH_4HCO_3 and 2 M urea before being digested by trypsin (0.6 μg/sample) overnight at 37 °C. The peptide mixture was acidified with 0.5% trifluoroacetic acid and fractionated using the High pH Reversed-Phase Peptide Fractionation Kit (Thermo Fisher Scientific) following the manufacturer's protocol. Peptides in each fraction (8/sample) were dried, resuspended in 2.5% acetonitrile 0.1% TFA and 0.1% formic acid and then analyzed by an UltiMate 3000 RSLCnano-LC system, (Thermo Fisher Scientific) connected on-line *via* a nano-ESI source to an Q Exactive plus™ Hybrid Quadrupole-Orbitrap™ Mass Spectrometer (Thermo Fisher Scientific). Each peptide mixture was separated on the analytical C18 column (PepMap™ RSLC C18, 150 mm × 75 μm, Thermo Fisher Scientific) using a 100 min multistep elution gradient from 4% to 90% of mobile phase B (0.1% formic acid in 80% ACN) at a constant flow rate of 300 nl/min. Eluted peptides were electrosprayed directly into the mass spectrometer with an ESI voltage of 2.0 kV. Mass spectrometry data were acquired in a positive mode using a data-dependent mode selecting the 15 most intense ions with the following parameters: full scan spectra range from *m/z* 350.0 to *m/z* 1,700.0, resolution of 70,000, injection time 100 ms, AGC target 3×10^6, isolation window ± 2.0 m/z and the dynamic exclusion 20 s. For HCD fragmentation, resolution was set to 17,500, AGC target to 10,000 and injection time to 80 ms. Proteins were automatically identified by MaxQuant (v. 1.6.17.0) software. Tandem mass spectra were searched against the *Homo sapiens* dataset of UniprotKB database (Release: Feb 2016; 550,552 sequences). Quantitative comparison among HDs and HCV T0/T6 was performed using the label-free quantification algorithm calculated by MaxQuant.

Statistical analysis

All statistical analyses were performed using GraphPad Prism 8 software. Data on LX2 cells were analyzed using Student's *t* tests. Mann-Whitney test and Wilcoxon's non-parametric test were applied for EV miRNA and protein content analysis. Perseus software (version 1.6.7.0) after log2 transformation of the intensity data was applied to proteomic study. Statistical analysis was carried out on proteins identified in 100% of the samples. Results were considered statistically significant at $p \leq 0.05$. To improve visualization, a z-score plot and a cluster heat map were generated. Gene ontology enrichment analysis of biological processes, molecular functions and cellular components were performed by PANTHER software using Fisher's exact test and applying the false discovery rate calculation as a correction for multiple testing.

Results

Functional analysis of circulating EVs

Previous studies characterized LX2 cells as similar to "activated HSCs"[13] that retain a transcriptional reprogramming plasticity in response to co-culture with hepatocytes.[14] Here, the properties of the EVs derived from non-tumorigenic hepatocyte cell lines were first tested on recipient LX2 cells and shown to induce a downregulation of fibrogenic markers (*i.e.* FN-1, ACTA2, COL1α1 and TGFβ1), thus providing proof that LX2 cells represent a suitable read out for EV functional studies. A comparison between these data and those obtained with EVs derived from the HepG2 tumoral cell line are shown in Fig. S1.

Incubation of LX2 with EVs derived from HD plasma results in a significant reduction of *FN-1, ACTA2, COL1α1, PAI-1* and *CTGF* mRNA expression levels compared to LX2 untreated cells (Fig. 1A). FN-1 and ACTA2 downregulation was also confirmed at the protein level (Fig. 1B). Moreover, ECM deposition, investigated by confocal analysis and shown in Fig. 1C, was reduced in LX2 cells treated with EVs derived from HD in comparison with non-treated cells.

Notably, HCV-derived EVs do not share this ability. As shown in Fig. 1D, the mRNA levels of the fibrogenic markers *FN-1, ACTA2, COL1α1* and *TGFβ1* are significantly higher in LX2 cells treated with T0 and T6 EVs compared to HD EVs. This observation has been confirmed at the protein level for FN-1, ACTA2 and for the p-SMAD2/3 (markers of TGFβ pathway activation) (Fig. 1E-F). Finally, ECM deposition has been investigated by confocal analysis; as shown in Fig. 1G, significant collagen deposition was observed in LX2 cells treated with T0 and T6 EVs, in striking contrast with what was observed with HD EVs (Fig. 1C).

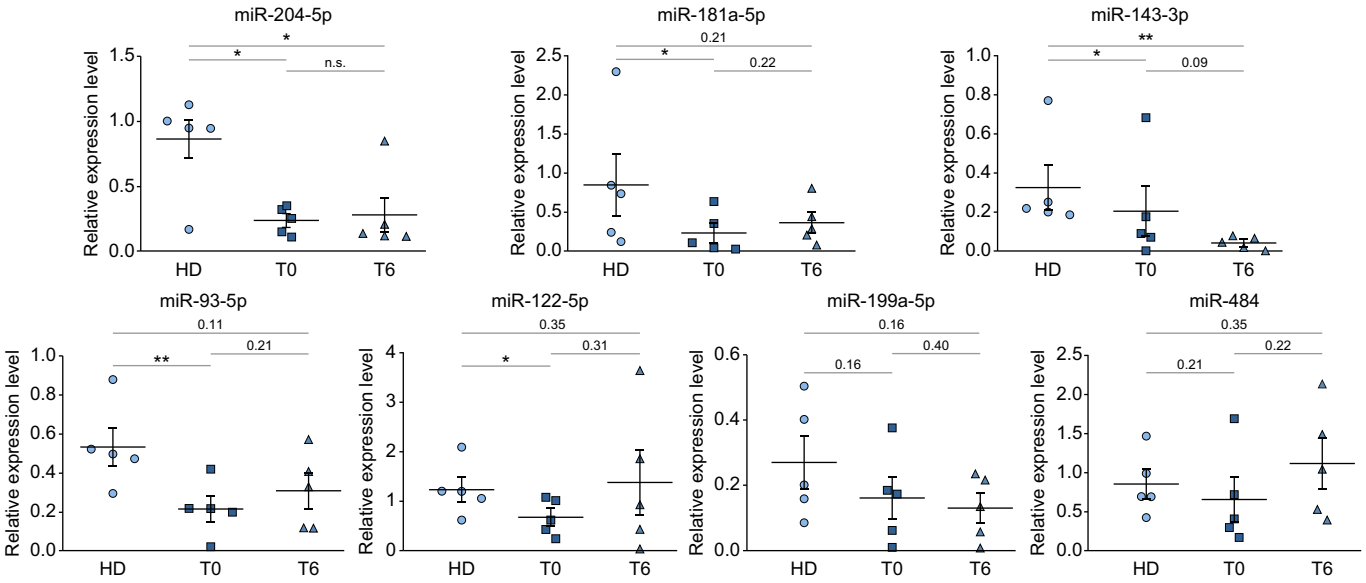

Fig. 2. HCV infection modifies the miRNA content of EVs. HD and HCV T0/T6 EVs were isolated from 1 ml plasma (n = 5). Expression of the indicated miRNAs was analyzed. Data are normalized to geometric mean of miR26a, miR22-5p and miR191 and are expressed as 2-(-ΔCt). Statistical analysis was performed by Mann-Whitney test (HD/T0 and HD/T6 comparison) and by Wilcoxon's test (T0/T6 comparison). p <0.05 is considered statistically significant. EVs, extracellular vesicles; HDs, healthy donors.

Table 2. Protein content-based EV characterization.

Transmembrane EV proteins			
Protein names	**Gene names**	**Peptides**	**Sequence coverage [%]**
Non-tissue specific			
Disintegrin and metalloproteinase domain-containing protein 10	*ADAM10*	27	44.1
Guanine nucleotide-binding protein subunit alpha-13	*GNA13*	18	57.3
Integrin alpha-5	*ITGA5*	14	19.2
CD59 glycoprotein	*CD59*	4	29.6
Integrin beta-3	*ITGB3*	37	54.8
Integrin beta-1	*ITGB1*	26	39.7
Integrin alpha-IIb	*ITGA2B*	45	48.6
Integrin alpha-6	*ITGA6*	52	56.1
MHC class I antigen	*HLA-B*	12	54.9
MHC class I antigen	*HLA-A*	19	55.9
Tissue/cell specific			
Platelet endothelial cell adhesion molecule	*PECAM1*	30	51.6
Tetraspanin CD9 antigen	*CD9*	5	33.3
Tetraspanin Leukocyte antigen CD37	*CD37*	3	18.1
Integrin alpha-IIb	*ITGA2B*	45	48.6
Cytosolic EV proteins			
Protein names	**Gene names**	**Peptides**	**Sequence coverage [%]**
With lipid or membrane protein-binding ability			
Syntenin-1	*SDCBP*	10	62.1
Annexin A7	*ANXA7*	17	47.9
Flotillin-1	*FLOT1*	11	33.7
Annexin A11	*ANXA11*	19	39
ADP-ribosylation factor 6	*ARF6*	7	60
Promiscuous incorporation in EVs			
Tubulin beta-4B chain	*TUBB4B*	22	66.1
Tubulin beta-1 chain	*TUBB1*	26	86

Only EV proteins identified in all the analyzed samples are listed. The abundance of EV-specific transmembrane markers in the analyzed samples is shown. The list includes non-tissue specific proteins (tetraspanins, ADAM 10, GNA13, MHC class I and Integrins), CD37 (specific for leukocytes), PECAM 1 (specific for endothelial cells). ESCRT I, II III complex and accessory proteins (CHMP4B VPS4B), flotillins, annexins, ARF6 and syntenin are considered incorporated into EVs.

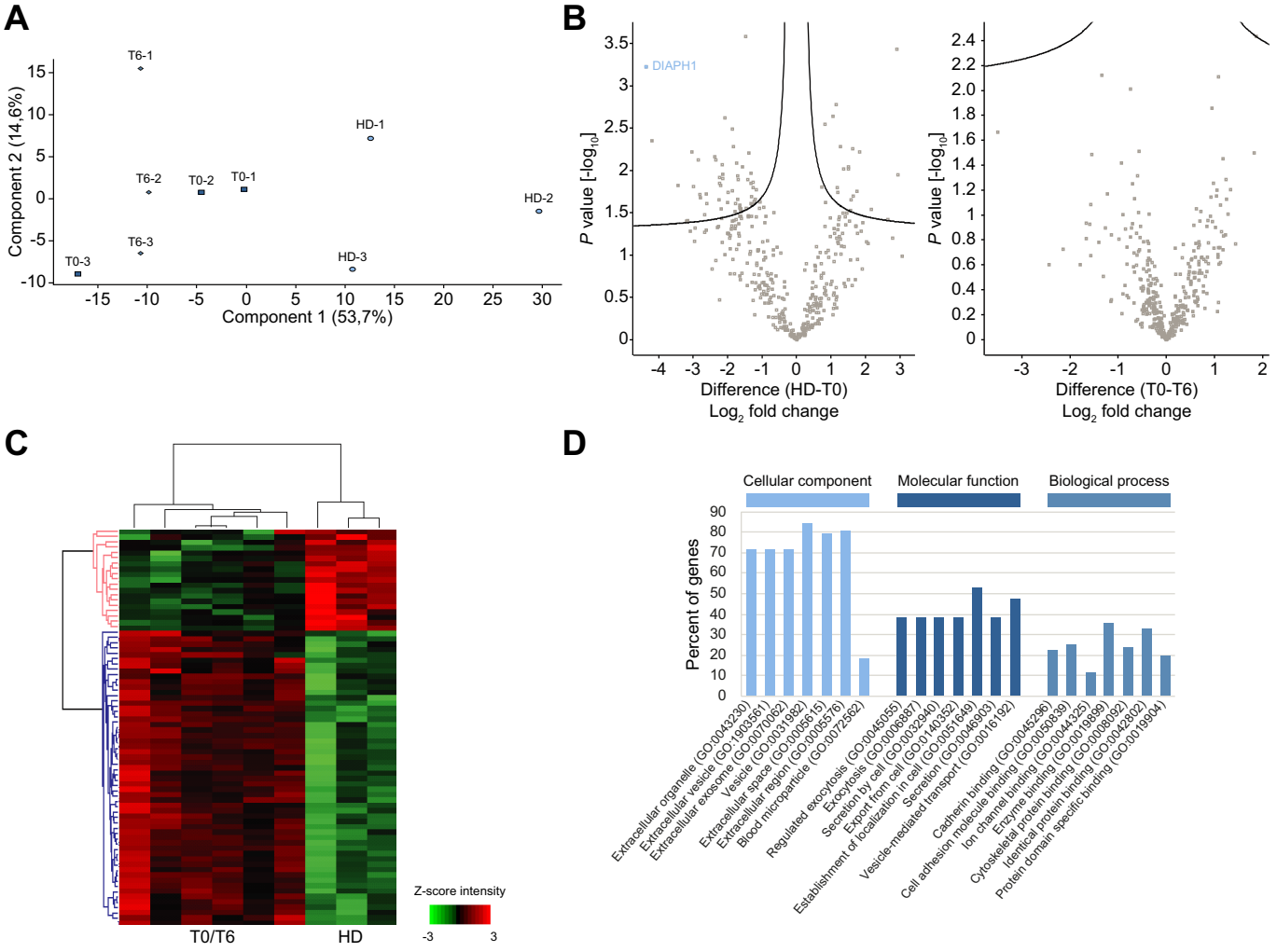

Fig. 3. HCV infection modifies the protein content of EVs. EVs were isolated from 1 ml plasma of enrolled HDs and from HCV patients before (T0) and after 6 months of DAA therapy (T6) (n = 3) and 15 ug of EV proteins per sample were analyzed by label-free liquid chromatography-mass spectrometry. (A) Principal component analysis of the label-free quantification intensities obtained in T0 (red squares), T6 (blue) and HD (black) datasets. (B) Volcano plots comparing HD *vs.* T0 (left panel) and T0 *vs.* T6 (right panel). Black curves represent the significance threshold at an FDR of 0.05 and S0 of 0.1. The top protein with the largest fold change between T0 and HD is labeled in the plot. (C) Heat map of 74 differentially expressed proteins in T0/T6 and HDs. Label-free quantification intensities were expressed in z-score values (range of intensity z-score: ±3). Upregulated and downregulated proteins are expressed in red and green scale, respectively. Hierarchical clustering was performed using Euclidean distance and average linkage using the Perseus software. (D) GO enrichment analysis performed by PANTHER software on 74 differentially expressed proteins between HDs and T0 datasets. The test type chosen was Fisher's exact test and the false discovery rate calculation was applied as a correction for multiple testing. DAA, direct-acting antiviral; EVs, extracellular vesicles; FDR, false discovery rate; GO, gene ontology; HDs, healthy donors.

Overall, these data provide evidence for an EV-mediated fibrotic stimulus in HCV patients and, notably, as highlighted by the longitudinal study, for its persistence in spite of DAA-mediated viral clearance (Table S1).

Structural analysis: miRNA content of circulating EVs

In order to correlate functional properties with structural evidence, we analyzed the miRNA informational cargo of EVs isolated from the plasma of the same HD and the same treatment-naïve, viraemic HCV patients. Indeed, different levels of fibrogenic markers may reflect the presence/absence of specific miRNAs with known antifibrogenic properties (listed in Table 1).

A crucial aspect for a qPCR analysis of these miRNAs has been the identification of miRNAs to be used as normalizing reference factors; to this end, taking advantage of previous findings, we used the geometric mean of miR26a, miR22-5p and miR191.[11,12]

Notably, EV analysis highlighted that miR204-5p,[15–17] miR181a-5p,[18,19] miR143-3p,[20,21] miR93-5p[22] and miR-122-5p[23,24] were statistically decreased in EVs from HCV-infected patients (T0) with respect to HDs. The same trend of reduction in infected patients was also found for miR199a-5p[25] and miR484,[26] although the results bear no significant differences (Fig 2). No statistically significant differences were found for the antifibrogenic miRNAs miR199a-3p,[27] miR486,[28] miR320a,[29,30] miR93-3p[31] and miR145-5p[32,33] (Fig. S3).

Next, miRNA analysis was extended to EVs isolated from the plasma of the same patients after 6 months of DAA therapy (T6). Consistent with functional analysis on the LX2 cell line, DAA treatment correlates with a statistical difference between HDs and DAA-treated patients for miR204-5p and miR143-3p, thus indicating that EV-mediated signals still lack antifibrogenic informational content in spite of viral eradication (Fig. 2). This

Table 3. Upregulated proteins identified in HCV-T0 and HD.

p value ($-\log_{10}$)	Difference HD-T0 ($\log_2$ fold-change)	Protein names	Gene names	Peptides	Unique peptides
Upregulated proteins identified in HCV-T0 (with respect to HD)					
3.23	-4.37	Protein diaphanous homolog 1	*DIAPH1*	33	33
2.35	-4.20	Ras GTPase-activating-like protein IQGAP2	*IQGAP2*	39	38
1.82	-3.43	Annexin A3	*ANXA3*	17	17
1.40	-3.19	Protein kinase C beta type	*PRKCB*	19	12
1.40	-3.16	Rho GTPase-activating protein 18	*ARHGAP18*	23	23
2.22	-3.04	6-phosphogluconate dehydrogenase	*PGD*	16	16
1.81	-2.99	Rho GTPase-activating protein 1	*ARHGAP1*	14	14
2.13	-2.85	Glucose-6-phosphate isomerase	*GPI*	15	1
1.71	-2.81	T-complex protein 1 subunit zeta	*CCT6A*	15	15
1.68	-2.79	EH domain-containing protein 1	*EHD1*	25	14
1.47	-2.66	Septin-6	*SEPT6*	11	6
1.72	-2.63	Platelet glycoprotein V	*GP5*	15	15
1.61	-2.61	WD repeat-containing protein 1	*WDR1*	23	23
2.16	-2.37	Cullin-associated NEDD8-dissociated protein 1	*CAND1*	16	16
2.13	-2.34	Platelet glycoprotein Ib beta chain	*GP1BB*	5	5
1.65	-2.25	Pyruvate kinase	*PKM*	34	4
1.92	-2.24	Platelet glycoprotein Ib alpha chain;Glycocalicin	*GP1BA*	12	1
1.85	-2.23	Adenylyl cyclase-associated protein;Adenylyl cyclase-associated protein 1	*CAP1*	22	1
1.82	-2.21	Platelet glycoprotein IX	*GP9*	5	5
1.54	-2.18	Crk-like protein	*CRKL*	9	9
2.07	-2.15	L-lactate dehydrogenase;L-lactate dehydrogenase B chain	*LDHB*	15	14
1.95	-2.14	L-lactate dehydrogenase;L-lactate dehydrogenase A chain	*LDHA*	14	13
1.91	-2.14	Actin-related protein 2	*ACTR2*	10	10
2.62	-2.08	Coronin-1A	*CORO1A*	15	15
1.62	-2.00	Heat shock protein HSP 90-alpha	*HSP90AA1*	29	19
1.74	-1.98	EH domain-containing protein 3	*EHD3*	30	18
1.76	-1.86	Phosphoglucomutase-1	*PGM1*	13	6
2.49	-1.86	Phosphoglycerate kinase;Phosphoglycerate kinase 1	*PGK1*	19	19
2.28	-1.83	Tubulin alpha-4A chain	*TUBA4A*	19	5
1.52	-1.78	Transgelin-2	*TAGLN2*	13	13
1.61	-1.77	Talin-1	*TLN1*	119	108
2.09	-1.74	Fructose-bisphosphate aldolase A	*ALDOA*	19	16
1.66	-1.71	Calmodulin	*CALM1*	8	7
1.94	-1.71	14-3-3 protein theta	*YWHAQ*	13	11
1.89	-1.69	Thymidine phosphorylase	*TYMP*	16	16
1.56	-1.65	Synaptotagmin-like protein 4	*SYTL4*	15	15
1.59	-1.64	Rab GDP dissociation inhibitor alpha	*GDI1*	20	13
1.55	-1.62	Tubulin alpha-1C chain	*TUBA1C*	19	2
1.52	-1.61	14-3-3 protein zeta	*YWHAZ*	15	12
1.55	-1.61	Filamin-A	*FLNA*	126	118
2.04	-1.57	Heat shock cognate 71 kDa protein	*HSPA8*	26	23
3.58	-1.48	Peroxiredoxin-6	*PRDX6*	16	16
1.55	-1.46	Tubulin alpha-8 chain	*TUBA8*	16	6
1.89	-1.41	14-3-3 protein beta	*YWHAB*	12	8
2.21	-1.38	Coagulation factor XIII A chain	*F13A1*	29	1
1.97	-1.33	Glyceraldehyde-3-phosphate dehydrogenase	*GAPDH*	17	17
1.85	-1.32	GTP-binding nuclear protein Ran	*RAN*	6	6
1.61	-1.31	14-3-3 protein eta	*YWHAH*	16	14
1.69	-1.31	Integrin alpha-2	*ITGA2*	30	6
1.59	-1.30	Tropomyosin alpha-3 chain	*TPM3*	16	5
1.86	-1.26	Triosephosphate isomerase	*TPI1*	14	14
1.80	-1.26	14-3-3 protein epsilon	*YWHAE*	21	19
1.63	-1.22	Guanine nucleotide-binding protein G(I)/G(S)/G(T) subunit beta-1	*GNB1*	15	9
1.66	-1.20	Rab GDP dissociation inhibitor beta	*GDI2*	20	13
1.77	-1.16	Alpha-enolase	*ENO1*	20	17
Upregulated proteins identified in HD (with respect to HCV-T0)					
1.95	2.94	Haptoglobin-related protein	*HPR*	22	6
3.44	2.92	Apolipoprotein L1	*APOL1*	13	13
1.42	2.66	Plasma kallikrein	*KLKB1*	23	22
1.54	2.18	Serum paraoxonase/arylesterase 1	*PON1*	11	11
2.22	1.84	Angiogenin	*ANG*	9	9
1.75	1.75	C4b-binding protein beta chain	*C4BPB*	6	6
1.70	1.65	Hyaluronan-binding protein 2	*HABP2*	20	20
2.26	1.63	Transthyretin	*TTR*	10	10
1.66	1.58	Complement component C8 beta chain	*C8B*	16	16

(*continued on next page*)

Table 3. (*continued*)

p value ($-\log_{10}$)	Difference HD-T0 ($\log_2$ fold-change)	Protein names	Gene names	Peptides	Unique peptides
1.53	1.57	Complement component C8 alpha chain	*C8A*	10	10
2.04	1.51	Inter-alpha-trypsin inhibitor heavy chain H4	*ITIH4*	36	1
2.02	1.51	Apolipoprotein C-III	*APOC3*	9	9
2.02	1.36	Vitronectin	*VTN*	17	17
2.28	1.28	Inter-alpha-trypsin inhibitor heavy chain H2	*ITIH2*	24	24
1.74	1.19	Plasminogen	*PLG*	38	33
1.80	1.18	Selenoprotein P	*SEPP1*	5	5
2.78	1.15	Complement C1r subcomponent	*C1R*	28	28
2.64	1.06	Vitamin K-dependent protein S	*PROS1*	16	16
2.55	0.83	C4b-binding protein alpha chain	*C4BPA*	23	2

HD, healthy donor; HCV-T0, patients with chronic HCV before treatment.

result is conceivably causally associated with the functional observation previously described, since both bioinformatic predictions and previous reports pinpoint these miRNAs as regulators of fibrogenic markers. In order to formally acquire mechanistic insights on each miRNA-specific role, an miRNA mimic-based analysis has been performed. miRNA mimic pool (miR204-5p, miR181a-5p, miR143-3p and miR93-5p) and each single miRNA mimic have been transfected into LX2 cells, and potential direct/indirect target mRNAs (FN-1, ACTA2, COL1α1, TGF-β1, TGF-βR1, CTGF) have been quantified. As shown in Fig. S4, this analysis provides functional evidence recapitulating the EV-based observation and enables identification of miRNA-specific targets (Table 1).

Taken together, these results indicate that circulating EVs derived from HDs, HCV-infected and DAA-treated patients have a different miRNA content. These differences could have a causal role in fibrosis progression despite viral clearance.

Structural analysis: circulating EV proteomic analysis

Next, we aimed to characterize EV protein content; to this end, EVs have been purified as above from 3 HDs and 3 HCV patients (at T0 and at T6). Following proteolytic digestion, proteins were extracted and separated in 8 fractions based on their hydrophobicity before being analyzed by label-free liquid chromatography-mass spectrometry. Several proteins have been found coherently expressed at the same level in all 9 samples (see Table 2). Among them, we identified 2 categories of EV markers in accordance with the "minimal experimental requirements for definition of EVs and their functions".[34] The first category includes transmembrane proteins localized on the plasma membrane and/or endosomes (*e.g.* CD9, CD37, CD59, ADAM 10, PECAM1, ITGA5, ITGA6 and ITGB1), while the second category consists of cytosolic proteins enclosed in EVs (*e.g.* FLOT-1, ANXA7, SDCBP). These results also provide evidence for the proper normalization among samples. Moreover ITGA5, found at the same levels in all samples, has been indicated to confer hepatotropism to EVs[35] and ADH, GST, HP, FGB unveil the hepatic origin of EVs (see supplementary material).

Next, in order to identify differentially expressed proteins among the 3 groups, computational analysis has been carried out; firstly, principal component analysis of 393 detected proteins indicated that HCV patients (T0-T6) are distributed in a distinct group from HDs (Fig. 3A). In the differential expression analysis comparing HDs to T0, 74/393 EV-associated proteins were found differentially expressed with a false discovery rate of <0.05 (19 expressed higher in control and 55 expressed higher in T0, see

Table 4. Protein gene ontology.

GO category	GO terms	Count in gene set	Raw *p* value	FDR
Cellular component				
	Extracellular organelle (GO:0043230)	54	3.19E-36	2.13E-33
	Extracellular vesicle (GO:1903561)	54	3.04E-36	3.05E-33
	Extracellular exosome (GO:0070062)	54	1.83E-36	3.67E-33
	Vesicle (GO:0031982)	64	1.45E-34	7.29E-32
	Extracellular space (GO:0005615)	60	4.54E-33	1.82E-30
Biological process				
	Regulated exocytosis (GO:0045055)	29	4.56E-23	7.26E-19
	Exocytosis (GO:0006887)	29	1.50E-21	1.19E-17
	Secretion by cell (GO:0032940)	29	4.83E-19	2.56E-15
	Export from cell (GO:0140352)	29	1.73E-18	6.86E-15
	Establishment of localization in cell (GO:0051649)	40	2.46E-18	7.81E-15
Molecular function				
	Cadherin binding (GO:0045296)	17	4.12E-15	1.96E-11
	Cell adhesion molecule binding (GO:0050839)	19	9.38E-14	2.23E-10
	Ion channel binding (GO:0044325)	9	2.92E-09	4.64E-06
	Enzyme binding (GO:0019899)	27	1.93E-08	1.83E-05
	Cytoskeletal protein binding (GO:0008092)	18	1.68E-08	1.99E-05

FDR, false discovery rate; GO, gene ontology.

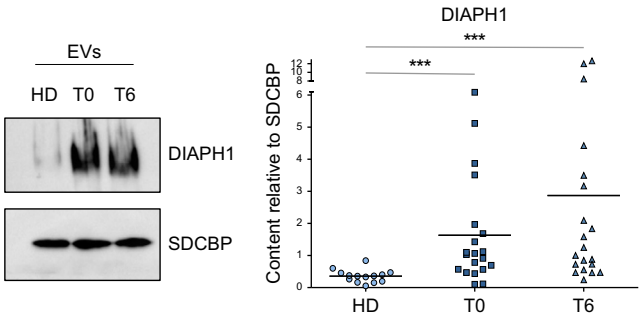

Fig. 4. Persistence of DIAPH1 in EVs from HCV patients despite viral eradication. Western blot and densitometric analysis of DIAPH1 in plasma-derived EVs from enrolled HDs (n = 14), T0/T6 (n = 20) patients. Syntenin 1 (SDCBP) was used as a loading control. Statistical analysis was performed by Mann-Whitney test (HD/T0 and HD/T6 comparison) and by Wilcoxon's test (T0/T6 comparison) p <0.05 is considered statistically significant. EVs, extracellular vesicles; HDs, healthy donors.

Table 3). Conversely, non-statistically significant differences in EV proteomic profile were observed between HCV patients before (T0) and after DAA treatment (T6) (Fig. 3B). Indeed, as for principal component analysis, hierarchical clustering classified the participants into only 2 groups based on differentially expressed proteins, one comprising both T0 and T6 datasets, and the other containing HDs. Heat map representation of these results is shown in Fig. 3C. Furthermore, gene ontology enrichment analysis of the 74 differentially expressed proteins in T0 compared to HDs is reported (Fig. 3D, Table 4). Among the proteins upregulated in T0, new potential biomarkers and therapeutic targets causal to liver disease progression could be present.

So far, we focused on the protein diaphanous homolog 1 (DIAPH1) belonging to the family of formin proteins and recently described to promote myofibroblastic activation of HSCs.[36–38] Indeed, this protein was found as the most upregulated in T0, and worthy of note, also in T6 samples despite viral clearance. With the intent to validate this evidence by means of a different approach and in order to extend it to a broader patient group, western blot analysis was performed on 14 HD and 20 longitudinally enrolled HCV patient (T0 and T6) EV samples. As shown in Fig. 4 and coherently with proteomic data, the level of DIAPH1 was significantly higher in T0 and T6 EVs compared to HD EVs. Taken together, these results provide evidence indicating that circulating EVs derived from HCV-infected and DAA-treated patients differ in protein composition with respect to HDs. Moreover, specific cargo content conceivably indicates a causal role for EVs in liver disease progression.

Overall, our data highlight a correlation between EV function and the miRNA and protein content of EVs, implicating EVs as relevant players in HCV-related pathogenesis. Our data shows a number of persistent modifications and should act as a warning that long-term fibrosis can still progress despite DAA-mediated viral clearance.

Discussion

The major result of our work is that it provides evidence on the impact of circulating EVs –derived from plasma of both HCV-infected (T0) and DAA-treated patients (T6) – on HSC trans-differentiation/activation. The comparison between HD-derived EVs and both T0 and T6-derived EVs highlighted functional differences correlating with structural EV properties. Functionally, EVs derived from HD plasma display an antifibrogenic ability (*i.e.* decrease of LX2 fibrogenic markers) that is lost by HCV T0/T6 EVs; coherently, HCV EVs stimulate SMAD2/3 phosphorylation and collagen deposition. These functional differences correlate with specific cargo signatures in terms of miRNAs and proteins.

Our data indicating that HCV-derived EVs can induce fibrogenic marker expression are in line with previous reports highlighting activation of LX2 upon HCV EV uptake. In particular, EVs were found to activate the TGFβ pathway (through miR19a and miR192).[39,40]

The antifibrogenic miRNAs miR204-5p, miR181a-5p, miR143-3p, miR93-5p and miR122-5p were decreased in viraemic HCV patients and miR204-5p and miR143-3p were decreased in DAA-treated patients compared to HDs. Previous studies have focused on the intracellular miRNA profile in relation to HCV infection.[41] Specifically, among the miRNAs associated with inflammation, fibrosis and cancer progression, miR143-3p appears to be upregulated in HCV-infected cells. This should not be considered in contrast with our results since it is well established that EV miRNA content does not reflect the cellular level of ncRNA and that specific RNA-binding proteins (RBPs) participate in specific miRNA EV-loading.[42,43] This combined evidence suggests the need to investigate the influence of HCV on RBP loading activity.

Data mining highlighted the following antifibrogenic miRNAs: miR-204-5p, predicted and experimentally validated to target TGFβ receptor II (TGFβRII)[15]; miR93-5p, described to downregulate FN-1 and ACTA2[22]; miR181a-5p, known to directly target TGFβ receptor I (TGFβRI)[18]; miR143-3p, described to impact ECM deposition (COL1α1, FN-1 and ACTA2).[20,21] Here, by means of a mimic-based approach, these data have been confirmed/extended. With respect to miR-122-5-p expression (that indicates that the plasma-derived purified EVs include those of hepatic origin) our data are in line with previous reports showing an inverse relationship between its expression and liver fibrosis..[23]

With respect to EV protein cargo, a proteomic-based approach pinpointed the liver pathogenetic protein DIAPH1, increased in both T0 and T6 EV datasets (log_2 fold change of 4.4) with respect to HD EVs. This latter result has been validated in a significant number of samples. DIAPH1 has a key role in myofibroblast differentiation and is involved in actin nucleation/elongation and ACTA2 induction.[37,38] Notably, it has recently been shown that DIAPH1 stimulates myofibroblastic activation of HSCs, promoting the endocytosis of TGFβRII[36]; it may also contribute to HSC activation by favoring the formation of ACTA2-positive stress fibers. Moreover, DIAPH1 inactivation suppresses HSCs' tumor-promoting effects in a tumor implantation mouse model.[36]

With respect to other HCV-induced EV hit proteins that could be potential biomarkers, it is worth noting that ANXA3 and ACTR2 have previously been described as poor prognostic signatures in HCV cirrhotic patients.[44] This evidence strongly supports the notion of persistent fibrogenic/pathogenic EV informational content despite viral clearance.

The risk of developing liver-related complications in DAA-treated patients reaching SVR is debated.[45] Interestingly, evidence has revealed that the liver fibrosis process is not unidirectional and permanent, but instead plastic and potentially reversible.[46–48] At the moment there are no "gold standard" therapies for liver fibrosis, and HSCs are now considered a main

drug target as highlighted by selective rilpivirine-mediated HSC ablation which can ameliorate liver fibrosis.[49]

In this context, circulating plasma and serum EV-content analysis could enable the monitoring of biomarkers (*e.g.* DIAPH1) associated with liver fibrosis, supporting the long-term monitoring and clinical management of patients.[50]

Recently, a quantitative proteomic analysis compared microparticles derived from the plasma of patients with HCV-induced cirrhosis and HCC to those from HDs[51]; none of their top modulated hits were shared with our dataset. This is conceivably because of the different origin of the biological material (*i.e.* different pathological conditions and different procedures of isolation for microparticles and EVs) and underlines the possibility of identifying new HCV-related biomarkers and therapeutic targets by means of specific cellular and extracellular compartment analysis. We cannot state that the structural evidence identified herein (specific miRNAs and proteins) confirms a causal role for these EV components in the pro-fibrogenic process. Nevertheless, we have gathered insights on the direct role of plasma-derived EVs from T0 and T6 patients in the pro-fibrotic process. Therefore, our functional and structural observations could contribute to the development of therapeutic approaches tailored for long-term management of patients reaching SVR by DAA treatment.

Abbreviations

DAA, direct-acting antiviral; DIAPH1, diaphanous homolog 1; EBV, Epstein-Barr virus; ECM, extracellular matrix; EVs, extracellular vesicles; HCC, hepatocellular carcinoma; HDs, healthy donors; HSC, hepatic stellate cells; miRNA/miR, microRNA; qPCR, quantitative PCR; SVR, sustained virological response.

Financial support

This study was funded by the EXO-DAA project, L.R. Lazio 13/08, Ministry for Health of Italy (Ricerca Corrente) and Sapienza University of Rome RG11916B6A9C42C7 (to M.T.), Italian Ministry of Health Ricerca Finalizzata GR-2013-02359524 to CM and TV, Consorzio Interuniversitario Biotecnologie: fellowship to MGP.

Conflict of interests

The authors declare no potential conflicts of interest.

Please refer to the accompanying ICMJE disclosure forms for further details.

Authors' contributions

C. Montaldo: Investigation, conceptualization, data curation, formal analysis, validation, investigation, visualization, methodology. M. Terri: data curation, conceptualization, formal analysis, validation, investigation, visualization, methodology. V. Riccioni: data curation, formal analysis, validation, investigation, visualization, methodology. C. Battistelli: data curation, formal analysis, validation, investigation, visualization, writing-original draft and editing. V. Bordoni: data curation, formal analysis, methodology. G.P D'Offizi: patients' management, clinical data analysis. M.G. Prado: data curation, formal analysis, validation and methodology. F. Trionfetti: investigation, visualization, methodology. T. Vescovo: data curation, formal analysis, validation, investigation, visualization, methodology. E. Tartaglia: data curation, methodology. R. Strippoli: supervision, visualization, editing original draft. C. Agrati: conceptualization, resources, funding acquisition, visualization, project administration. M. Tripodi: conceptualization, resources, supervision, funding acquisition, visualization, writing-original draft, project administration and editing.

Data availability statement

The mass spectrometry proteomics data have been deposited to the ProteomeXchange Consortium via the PRIDE [52] partner repository with the dataset identifier PXD026869.

Supplementary data

Supplementary data to this article can be found online at https://doi.org/10.1016/j.jhep.2021.07.003.

References

Author names in bold designate shared co-first authorship

[1] World Health Organization. Global hepatitis report 2017. [cited 10 January 2021]. Available from: https://www.who.int/hepatitis/publications/global-hepatitis-report2017/en/.
[2] Park H, Wang W, Henry L, Nelson DR. Impact of all-oral direct-acting antivirals on clinical and economic outcomes in patients with chronic hepatitis C in the United States. Hepatology 2019;69:1032–1045. https://doi.org/10.1002/hep.30303.
[3] Pons M, Rodríguez-Tajes S, Esteban JI, Mariño Z, Vargas V, Lens S, et al. Non-invasive prediction of liver-related events in patients with HCV-associated compensated advanced chronic liver disease after oral antivirals. J Hepatol 2020;72:472–480. https://doi.org/10.1016/j.jhep.2019.10.005.
[4] Calvaruso V, Craxì A. Hepatic benefits of HCV cure. J Hepatol 2020;73:1548–1556. https://doi.org/10.1016/j.jhep.2020.08.006.
[5] De Re V, Caggiari L, De Zorzi M, Fanotto V, Miolo G, Puglisi F, et al. Epstein-Barr virus BART microRNAs in EBV- associated Hodgkin lymphoma and gastric cancer. Infect Agent Canc 2020;15:42. https://doi.org/10.1186/s13027-020-00307-6.
[6] Chettimada S, Lorenz DR, Misra V, Dillon ST, Reeves RK, Manickam C, et al. Exosome markers associated with immune activation and oxidative stress in HIV patients on antiretroviral therapy. Sci Rep 2018;8. https://doi.org/10.1038/s41598-018-25515-4.
[7] Santangelo L, Bordoni V, Montaldo C, Cimini E, Zingoni A, Battistelli C, et al. Hepatitis C virus direct-acting antivirals therapy impacts on extracellular vesicles microRNAs content and on their immunomodulating properties. Liver Int 2018;38:1741–1750. https://doi.org/10.1111/liv.13700.
[8] Tsuchida T, Friedman SL. Mechanisms of hepatic stellate cell activation. Nat Rev Gastroenterol Hepatol 2017;14:397–411. https://doi.org/10.1038/nrgastro.2017.38.
[9] Khomich O, Ivanov AV, Bartosch B. Metabolic hallmarks of hepatic stellate cells in liver fibrosis. Cells 2019;9. https://doi.org/10.3390/cells9010024.
[10] **Conigliaro A**, **Amicone L**, Costa V, De Santis Puzzonia M, Mancone C, Sacchetti B, et al. Evidence for a common progenitor of epithelial and mesenchymal components of the liver. Cell Death Differ 2013;20:1116–1123. https://doi.org/10.1038/cdd.2013.49.
[11] **Schwarzenbach H**, **Da Silva AM**, Calin G, Pantel K. Data normalization strategies for microRNA quantification. Clin Chem 2015;61:1333–1342. https://doi.org/10.1373/clinchem.2015.239459.
[12] Vandesompele J, De Preter K, Pattyn F, Poppe B, Van Roy N, De Paepe A, et al. Accurate normalization of real-time quantitative RT-PCR data by geometric averaging of multiple internal control genes. Genome Biol 2002;3. https://doi.org/10.1186/gb-2002-3-7-research0034.
[13] Xu L, Hui AY, Albanis E, Arthur MJ, O'Byrne SM, Blaner WS, et al. Human hepatic stellate cell lines, LX-1 and LX-2: new tools for analysis of hepatic fibrosis. Gut 2005;54:142–151. https://doi.org/10.1136/gut.2004.042127.
[14] Coulouarn C, Corlu A, Glaise D, Guénon I, Thorgeirsson SS, Clément B. Hepatocyte-stellate cell cross-talk in the liver engenders a permissive inflammatory microenvironment that drives progression in hepatocellular carcinoma. Canc Res 2012;72:2533–2542. https://doi.org/10.1158/0008-5472.CAN-11-3317.
[15] Yu H, Xu M, Dong Y, Liu J, Li Y, Mao W, et al. 1,25(OH) 2 D 3 attenuates pulmonary arterial hypertension via microRNA-204 mediated Tgfbr2/Smad signaling. Exp Cell Res 2018;362:311–323. https://doi.org/10.1016/j.yexcr.2017.11.032.

[16] Liang C, Yang Y, Guan J, Lv T, Qu S, Fu Q, et al. LncRNA UCA1 sponges miR-204-5p to promote migration, invasion and epithelial-mesenchymal transition of glioma cells via upregulation of ZEB1. Pathol Res Pract 2018;214:1474–1481. https://doi.org/10.1016/j.prp.2018.07.036.
[17] **Wang FE**, **Zhang C**, Maminishkis A, Dong L, Zhi C, Li R, et al. MicroRNA-204/211 alters epithelial physiology. FASEB J 2010;24:1552–1571. https://doi.org/10.1096/fj.08-125856.
[18] Guo D, Ye Y, Qi J, Zhang L, Xu L, Tan X, et al. MicroRNA-181a-5p enhances cell proliferation in medullary thymic epithelial cells via regulating TGF-β signaling. Acta Biochim Biophys Sin (Shanghai) 2016;48:840–849. https://doi.org/10.1093/abbs/gmw068.
[19] Liu L, Wang Y, Fan H, Zhao X, Liu D, Hu Y, et al. MicroRNA-181a regulates local immune balance by inhibiting proliferation and immunosuppressive properties of mesenchymal stem cells. Stem Cells 2012;30:1756–1770. https://doi.org/10.1002/stem.1156.
[20] **Cheng W**, **Yan K**, Xie LY, Chen F, Yu HC, Huang YX, et al. MiR-143-3p controls TGF-β1-induced cell proliferation and extracellular matrix production in airway smooth muscle via negative regulation of the nuclear factor of activated T cells 1. Mol Immunol 2016;78:133–139. https://doi.org/10.1016/j.molimm.2016.09.004.
[21] Mu S, Kang B, Zeng W, Sun Y, Yang F. MicroRNA-143-3p inhibits hyperplastic scar formation by targeting connective tissue growth factor CTGF/CCN2 via the Akt/mTOR pathway. Mol Cell Biochem 2016;416:99–108. https://doi.org/10.1007/s11010-016-2699-9.
[22] Ma J, Zhang L, Hao J, Li N, Tang J, Hao L. Up-regulation of microRNA-93 inhibits TGF-β1-induced EMT and renal fibrogenesis by down-regulation of Orai1. J Pharmacol Sci 2018;136:218–227. https://doi.org/10.1016/j.jphs.2017.12.010.
[23] Trebicka J, Anadol E, Elfimova N, Strack I, Roggendorf M, Viazov S, et al. Hepatic and serum levels of miR-122 after chronic HCV-induced fibrosis. J Hepatol 2013;58:234–239. https://doi.org/10.1016/j.jhep.2012.10.015.
[24] Matsuura K, De Giorgi V, Schechterly C, Wang RY, Farci P, Tanaka Y, et al. Circulating let-7 levels in plasma and extracellular vesicles correlate with hepatic fibrosis progression in chronic hepatitis C. Hepatology 2016;64:732–745. https://doi.org/10.1002/hep.28660.
[25] **Chen L**, **Chen R**, Velazquez VM, Brigstock DR. Fibrogenic signaling is suppressed in hepatic stellate cells through targeting of connective tissue growth factor (CCN2) by cellular or exosomal MicroRNA-199a-5p. Am J Pathol 2016;186:2921–2933. https://doi.org/10.1016/j.ajpath.2016.07.011.
[26] El-Maraghy SA, Adel O, Zayed N, Yosry A, El-Nahaas SM, Gibriel AA. Circulatory miRNA-484, 524, 615 and 628 expression profiling in HCV mediated HCC among Egyptian patients; implications for diagnosis and staging of hepatic cirrhosis and fibrosis. J Adv Res 2020;22:57–66. https://doi.org/10.1016/j.jare.2019.12.002.
[27] Zhang HY, Li CH, Wang XC, Luo YQ, Cao XD, Chen JJ. MiR-199 inhibits EMT and invasion of hepatoma cells through inhibition of Snail expression. Eur Rev Med Pharmacol Sci 2019;23:7884–7891. https://doi.org/10.26355/eurrev_201909_18998.
[28] **Chen T**, **Zhu J**, Cai T, Du W, Zhang Y, Zhu Q, et al. Suppression of non-small cell lung cancer migration and invasion by hsa-MIR-486-5p via the TGF-β/SMAD2 signaling pathway. J Canc 2019;10:6014–6024. https://doi.org/10.7150/jca.35017.
[29] **Chen C**, **Wang Y**, **Yang S**, Li H, Zhao G, Wang F, et al. MiR-320a contributes to atherogenesis by augmenting multiple risk factors and down-regulating SRF. J Cell Mol Med 2015;19:970–985. https://doi.org/10.1111/jcmm.12483.
[30] **Chou LF**, **Chen CY**, Yang WH, Chen CC, Chang JL, Leu YL, et al. Suppression of hepatocellular carcinoma progression through FOXM1 and EMT inhibition via hydroxygenkwanin-induced miR-320a expression. Biomolecules 2020;10. https://doi.org/10.3390/biom10010020.
[31] **Lyu X**, **Fang W**, **Cai L**, **Zheng H**, Ye Y, Zhang L, et al. TGFβR2 is a major target of miR-93 in nasopharyngeal carcinoma aggressiveness. Mol Canc 2014;13. https://doi.org/10.1186/1476-4598-13-51.
[32] Shen W, Wang Y, Wang D, Zhou H, Zhang H, Li L. miR-145-5p attenuates hypertrophic scar via reducing Smad2/Smad3 expression. Biochem Biophys Res Commun 2019;521. https://doi.org/10.1016/j.bbrc.2019.11.040.
[33] Zhou D dan, Wang X, Wang Y, Xiang XJ, Liang ZC, Zhou Y, et al. MicroRNA-145 inhibits hepatic stellate cell activation and proliferation by targeting ZEB2 through Wnt/β-catenin pathway. Mol Immunol 2016;75:151–160. https://doi.org/10.1016/j.molimm.2016.05.018.
[34] Théry C, Witwer KW, Aikawa E, Alcaraz MJ, Anderson JD, Andriantsitohaina R, et al. Minimal information for studies of extracellular vesicles 2018 (MISEV2018): a position statement of the International Society for Extracellular Vesicles and update of the MISEV2014 guidelines. J Extracell Vesic 2018;7. https://doi.org/10.1080/20013078.2018.1535750.
[35] **Hoshino A**, **Costa-Silva B**, Shen TL, Rodrigues G, Hashimoto A, Tesic Mark M, et al. Tumour exosome integrins determine organotropic metastasis. Nature 2015;527:329–335. https://doi.org/10.1038/nature15756.
[36] Liu D, Fu X, Wang Y, Wang X, Wang H, Wen J, et al. Protein diaphanous homolog 1 (Diaph1) promotes myofibroblastic activation of hepatic stellate cells by regulating Rab5a activity and TGFβ receptor endocytosis. FASEB J 2020;34:7345–7359. https://doi.org/10.1096/fj.201903033R.
[37] Chan MWC, Chaudary F, Lee W, Copeland JW, Mcculloch CA. Force-induced myofibroblast differentiation through collagen receptors is dependent on mammalian diaphanous (mDia) *. 2010. https://doi.org/10.1074/jbc.M109.075218.
[38] Li Y, Jiang G, Chen L, Jiang Y, Jiao J. Formin mDia1 contributes to migration and epithelial-mesenchymal transition of tubular epithelial cells exposed to TGF-β1. J Cell Biochem 2020;121:3861–3870. https://doi.org/10.1002/jcb.29508.
[39] Devhare PB, Sasaki R, Shrivastava S, Di Bisceglie AM, Ray R, Ray RB. Exosome-mediated intercellular communication between hepatitis C virus-infected hepatocytes and hepatic stellate cells. J Virol 2017;91. https://doi.org/10.1128/jvi.02225-16.
[40] Kim JH, Lee CH, Lee SW. Exosomal transmission of MicroRNA from HCV replicating cells stimulates transdifferentiation in hepatic stellate cells. Mol Ther - Nucleic Acids 2019;14:483–497. https://doi.org/10.1016/j.omtn.2019.01.006.
[41] Bandiera S, Pernot S, El Saghire H, Durand SC, Thumann C, Crouchet E, et al. Hepatitis C virus-induced upregulation of MicroRNA miR-146a-5p in hepatocytes promotes viral infection and deregulates metabolic pathways associated with liver disease pathogenesis. J Virol 2016;90:6387–6400. https://doi.org/10.1128/jvi.00619-16.
[42] **Mittelbrunn M**, **Gutiérrez-Vázquez C**, Villarroya-Beltri C, González S, Sánchez-Cabo F, González MÁ, et al. Unidirectional transfer of microRNA-loaded exosomes from T cells to antigen-presenting cells. Nat Commun 2011;2. https://doi.org/10.1038/ncomms1285.
[43] **Santangelo L**, **Giurato G**, Cicchini C, Montaldo C, Mancone C, Tarallo R, et al. The RNA-binding protein SYNCRIP is a component of the hepatocyte exosomal machinery controlling MicroRNA sorting. Cell Rep 2016;17:799–808. https://doi.org/10.1016/j.celrep.2016.09.031.
[44] Hoshida Y, Villanueva A, Sangiovanni A, Sole M, Hur C, Andersson KL, et al. Prognostic gene expression signature for patients with hepatitis C-related early-stage cirrhosis. Gastroenterology 2013;144:1024–1030. https://doi.org/10.1053/j.gastro.2013.01.021.
[45] Roche B, Coilly A, Duclos-Vallee JC, Samuel D. The impact of treatment of hepatitis C with DAAs on the occurrence of HCC. Liver Int 2018;38:139–145. https://doi.org/10.1111/liv.13659.
[46] Campana L, Iredale JP. Regression of liver fibrosis. Semin Liver Dis 2017;37:1–10. https://doi.org/10.1055/s-0036-1597816. Thieme Medical Publishers, Inc.
[47] Higashi T, Friedman SL, Hoshida Y. Hepatic stellate cells as key target in liver fibrosis. Adv Drug Deliv Rev 2017;121:27–42. https://doi.org/10.1016/j.addr.2017.05.007.
[48] Zoubek ME, Trautwein C, Strnad P. Reversal of liver fibrosis: from fiction to reality. Best Pract Res Clin Gastroenterol 2017;31:129–141. https://doi.org/10.1016/j.bpg.2017.04.005.
[49] Martí-Rodrigo A, Alegre F, Moragrega ÁB, García-García F, Martí-Rodrigo P, Fernández-Iglesias A, et al. Rilpivirine attenuates liver fibrosis through selective STAT1-mediated apoptosis in hepatic stellate cells. Gut 2020;69:920–932. https://doi.org/10.1136/gutjnl-2019-318372.
[50] Chen L, Brenner DA, Kisseleva T. Combatting fibrosis: exosome-based therapies in the regression of liver fibrosis. Hepatol Commun 2018;3. https://doi.org/10.1002/hep4.1290.
[51] Taleb RSZ, Moez P, Younan D, Eisenacher M, Tenbusch M, Sitek B, et al. Quantitative proteome analysis of plasma microparticles for the characterization of HCV-induced hepatic cirrhosis and hepatocellular carcinoma. Proteomics - Clin Appl 2017;11:1700014. https://doi.org/10.1002/prca.201700014.
[52] Perez-Riverol Y, Csordas A, Bai J, Bernal-Llinares M, Hewapathirana S, Kundu DJ. The PRIDE database and related tools and resources in 2019: improving support for quantification data. Nucl Acid Res 2019.